JYX
JYVÄSKYLÄN YLIOPISTO
UNIVERSITY OF JYVÄSKYLÄ

This is a self-archived version of an original article. This version may differ from the original in pagination and typographic details.

Author(s): Nissinen, J.; Heikkilä, T. T.; Volovik, G. E.

Title: Topological polarization, dual invariants, and surface flat bands in crystalline insulators

Year: 2021

Version: Published version

Copyright: ©2021 American Physical Society

Rights: In Copyright

Rights url: http://rightsstatements.org/page/InC/1.0/?language=en

Please cite the original version:

Nissinen, J., Heikkilä, T.T., & Volovik, G. E. (2021). Topological polarization, dual invariants, and surface flat bands in crystalline insulators. Physical Review B, 103(24), Article 245115. https://doi.org/10.1103/PhysRevB.103.245115

Topological polarization, dual invariants, and surface flat bands in crystalline insulators

J. Nissinen [1], T. T. Heikkilä [2], and G. E. Volovik [1,3]

[1] *Low Temperature Laboratory, Aalto University, P.O. Box 15100, FI-00076 Aalto, Finland*

[2] *Department of Physics and Nanoscience Center, University of Jyväskylä, P.O. Box 35 (YFL), FI-40014 University of Jyväskylä, Finland*

[3] *Landau Institute for Theoretical Physics, acad. Semyonov av., 1a, 142432 Chernogolovka, Russia*

(Received 9 September 2020; accepted 20 May 2021; published 11 June 2021)

We describe a crystalline topological insulator (TI) phase of matter that exhibits spontaneous polarization in arbitrary dimensions. The bulk polarization response is constructed by coupling the system to geometric deformations of the underlying crystalline order, represented by local lattice vectors—the elasticity tetrads. This polarization results from the presence of (approximately) flat bands on the surface of such TIs. These flat bands are a consequence of the bulk-boundary correspondence of polarized topological media, and contrary to related nodal line semimetal phases also containing surface flat bands, they span the entire surface Brillouin zone. We also present an example Hamiltonian exhibiting a Lifshitz transition from the nodal line phase to the TI phase with polarization. In addition, we discuss a general classification of three-dimensional (3D) crystalline TI phases and invariants in terms of the elasticity tetrads. The phase with polarization naturally arises from this classification as a dual to the previously better-known 3D TI phase exhibiting quantum (spin) Hall effect. Besides polarization, another implication of the large surface flat band is the susceptibility to interaction effects such as superconductivity: The mean-field critical temperature is proportional to the size of the flat bands, and this type of system may hence exhibit superconductivity with a very high critical temperature.

DOI: 10.1103/PhysRevB.103.245115

I. INTRODUCTION

The best-known topological insulators [1] in two dimensions are characterized by robust edge states and a (spin) Hall conductivity [2] quantized in the units of $\sigma_0 = e^2/h$. In three dimensions, conductivity scales like $\sigma_0/[\ell]$, where $[\ell]$ is a length scale characteristic to the system under consideration. In crystalline matter, the relevant length scale is obtained from the lattice vectors [3,4] and the quasitopological quantum Hall response is sensitive to geometry, being different in different directions specified by the reciprocal lattice vectors.

Another type of a quasitopological response is the electric polarization in arbitrary dimensions, being genuinely topological only in one dimension. It has been discussed, e.g., in Refs. [5–10], and has recently attracted renewed interest [11–19]. In 3D, the response is defined by the polarization charge density that scales like $1/[\ell^2]$. As we discuss in this paper, the multiplicative prefactor of the bulk response can still be quantized when suitably defined in terms of lattice geometry, as in 3D QH effect [20]. In crystalline media we may hence expect the relevant length scales to be associated with the crystal lattice vectors.

A natural framework to describe the interplay of topological response and lattice geometry in crystalline media is in terms of local lattice vectors $E_\mu^{\ a} = \partial_\mu X^a$—the elasticity tetrads (vielbein in general dimensions) [20–22], where the elastic embedding $X^a(x)$ counts the number of lattice planes in (laboratory) space along crystal direction a. They are a convenient way to discuss semiclassical hydrodynamics, elastic deformations, and conserved charges in terms of (continuum) lattice geometry [21]. Different from the dimensionless tetrads in the first order formulation of general relativity, they have the canonical dimensions of inverse length inherited from the underlying lattice. More recently, they have been shown to enter the field theoretical topological response of crystalline insulators with additional conserved lattice charges, specified by integer quantized momentum space invariants [19,20], and they can be extended [23] to the relativistic quantum fields and gravity [24–29]. In these cases, the associated crystal lattice is not necessarily due to periodic real space structure on which the fermionic system is placed but can be induced by interactions and/or other superstructures in the relevant ground state [30].

Here we show that using a combination of the elasticity tetrads $E_\mu^{\ a}$ and the electromagnetic gauge fields A_μ, one can in $3+1$ dimensions construct four different types of topological terms in the electromagnetic action. They are presented in Eqs. (5), (7), (9), and (13) and correspond to geometrically dual responses containing different numbers of elasticity tetrads: three and zero or one and two elasticity tetrads, respectively. As we discuss in Sec. II B, the first two describe the trivial band insulator and axion electrodynamics, respectively. The second pair describes the 3D quantum Hall (QH) effect [20] and topological polarization, which is the main focus in this paper. The QH and polarization responses and their dual relation in terms of the geometry of lattice vectors and planes are schematically described in Fig. 1.

The topological responses with elasticity tetrads give concrete examples of the crystalline insulators studied and classified in Refs. [12,32–35]. One formal distinction of our

 ©2021 American Physical Society

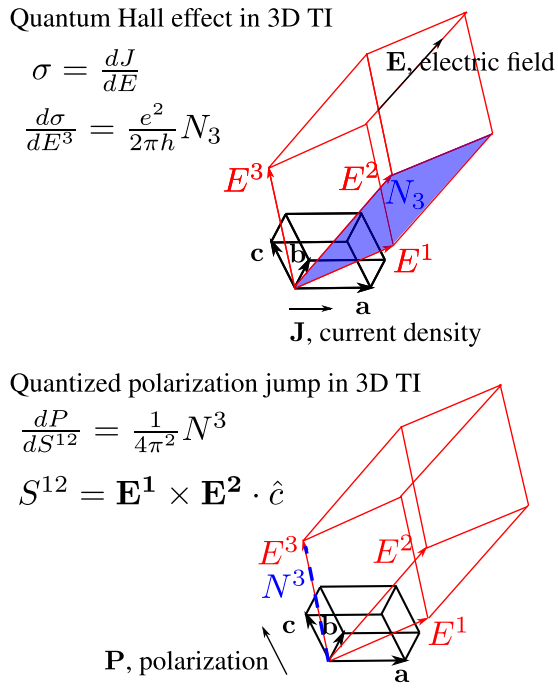

FIG. 1. Elementary cells of a crystal in real (spanned by **a**, **b**, **c**) and reciprocal spaces (E^a). Quantum Hall effect [2,31] is determined by the topological charge N_a integrated over the surface spanned by a pair of E^a, whereas the polarization jump is described by the charge N^a integrated along one E^a.

approach to the classification of crystalline topological phases is that only translational symmetries are necessary and the responses arise also in quasicrystals via higher dimensional lattice projections [22,36].

Besides quantized bulk polarization, the TI phase with polarization implies protected boundary modes. There is a marked difference between the boundary modes of the QHE-type topological insulators and those exhibiting surface polarization. Namely, whereas the previous form chiral "half-Dirac" surface modes [37], the surface states in the latter case form approximate flat bands spanning the entire surface Brillouin zone (BZ). Similar flat bands are found in the surfaces of nodal line semimetals [38–41], nodal line superconductors [42], and superfluids [43]. However, in those cases the flat bands span only part of the surface BZ, corresponding to the projection of the nodal lines to the surface.

Accordingly, here we discuss the topological polarization and flat band using an extension of a simple model [38] to the range of parameters relevant for crystalline insulators (or superconductors). In this extension the multiple Dirac points in a layered quasi-2D system evolve into a flat band, which occupies the whole 2D BZ on the boundaries of the 3D system when the number of atomic layers increases. This is accompanied by the formation of a topological crystalline insulator state in the bulk. In the numerical model, we consider the topological response and the corresponding topological invariants for the bulk topological insulator in terms of the elasticity tetrads and calculate the generalized polarization, matching the polarization by the surface flat bands.

II. TOPOLOGICAL POLARIZATION AND DUAL INVARIANTS IN CRYSTALLINE INSULATORS

In this section, we first review the elasticity tetrads, following Ref. [20], representing continuum translational gauge fields in the crystalline system. We then discuss the dual forms of topological responses arising from the elasticity tetrads in crystalline insulators in three dimensions. The duality is in the sense of the lattice volume and its lower dimensional subsystem volumes, counting the number of elasticity tetrads appearing. These are, respectively, the total (lattice) charge conservation and theta term, and, the three-dimensional quantum Hall effect and topological polarization. We assume a crystalline insulator with integer filling per band (without spin). Although charge transport is suppressed by the (mobility) gap in such insulators, the system is not strictly speaking gapped since e.g. the elasticity tetrads explicitly include symmetry breaking Goldstone modes. This carries over to the responses that are quantized in terms of the invariants and combinations of elasticity tetrads. Throughout the paper, we work mostly in units where $\hbar = e = 1$.

A. Elasticity tetrads

Let us consider the theory of crystalline elasticity using the approach of Refs. [20,21], which we now briefly review. An arbitrary, weakly deformed crystal structure can be described as a system of three crystallographic surfaces, the Bragg planes, of constant phase $X^a(x) = 2\pi n^a$, $n^a \in \mathbb{Z}$ with $a = 1, 2, 3$. The intersection of the surfaces

$$X^1(\mathbf{r}, t) = 2\pi n^1, \;\; X^2(\mathbf{r}, t) = 2\pi n^2, \;\; X^3(\mathbf{r}, t) = 2\pi n^3, \quad (1)$$

represent the lattice points of a deformed crystal in terms of an embedding. The embedding of the lattice points of the (electronic) crystal L in coordinate space is defined in terms of the inverse functions

$$L = \{\mathbf{R} = \mathbf{r}(n^a) | n^a \in \mathbb{Z}^3\}.$$

Although the lattice is always labeled by the integer (mod 2π) functions X^a, the embbedding in coordinate space can describe arbitrary (small) deformations. The integer lattice points can be shifted, $X^a \sim X^a + 2\pi$ without changing the physical lattice, so the periodic scalars X^a themselves cannot enter the physical response. Instead, their derivatives representing local lattice vectors can appear. These tangent vectors were termed elasticity tetrads (in three spatial dimensions) in Ref. [20]. In the continuum limit and three spatial dimensions, the elasticity tetrads are gradients of the phase functions:

$$\mathbf{E}^a = E_i{}^a(x) = \partial_i X^a(x) \quad i = x, y, z, \quad a = 1, 2, 3, \quad (2)$$

giving the local lattice vectors of a spatial crystal. In the simplest undeformed case, $X^a(x) = \mathbf{K}^a \cdot \mathbf{r}$, where $\mathbf{K}^a$ are the (primitive) reciprocal lattice vectors.

For simplicity, we work with the orthorhombic unit cell lattice system, but the generalization to other lattice symmetries and non-Bravais bases is in principle straightforward and does not affect the general results; a formal requirement of the responses we discuss is that field gradients are small at lattice scale. As a result, the elasticity tetrads refer to quantities averaged over the unit cell and our formulas are not sublattice

specific. We return to this briefly in Sec. IV. Generalizing to temporal directions, in an equilibrium (spacetime) crystal lattice the quantities $E_\mu{}^a$ are lattice four-vectors of the reciprocal (four-dimensional) Bravais lattice. Here E_t^a would describe dynamic changes in the lattice, such as phonons, whereas E_μ^0 would correspond to a periodicity in time. In what follows, we concentrate on the static case, but the formulas are readily generalizable to the dynamic case as well. In a deformed crystal, but in the absence of dislocations, the tetrads E_μ^a satisfy the integrability condition of vanishing torsion [20]

$$T_{\mu\nu}^a = \partial_\nu E_\mu{}^a - \partial_\mu E_\nu{}^a = 0. \tag{3}$$

In the absence of torsion, the embedding is globally well defined and single valued. The elasticity tetrads have dimension of inverse length, $[E_\mu^a] = 1/[l]$, being gradients of dimensionless scalars X^a. This and the presence of finite lattice symmetries is the main difference for the dimensionless tetrads used in the theories of general relativity. However, also in some theories of gravity, the tetrads have naturally dimension $1/[l]$, see, e.g., Refs. [23–29].

Due to the periodicity of the crystal, the scalar functions X^a play the role of continuum $U(1)$ fields, and thus the tetrads E_μ^a play the role of tautological vector potentials, i.e., effective gauge fields with torsion $T_{\mu\nu}^a$ as their field strength. When Eq. (3) holds, they imply conserved lattice charges along the different lattice sections a. In a crystalline topological insulator/superconductor, their antisymmetric tensor products correspond to higher-form conserved currents related to conserved particle numbers measured on lower-dimensional lattice sections [44]. In three dimensions, this emergent charge conservation occurs below the mobility/quasiparticle gap of the insulator/superconductor and is therefore only valid at low enough energies compared to the gap. For more details about these symmetries and the topological responses, see Ref. [44].

When the ordinary electric charge response is combined with elasticity tetrads, the bulk state can still have a (weak) topologically nontrivial subdimensional electromagnetic response with associated nonzero and quantized momentum space invariants. For similar ideas, see Refs. [45,46]. The "missing" elasticity tetrad fields enter in new crystalline topological terms and contain a mixture of the electromagnetic A_μ and elastic E_μ^a gauge fields [44], as we discuss next.

B. Lattice volume and 3D theta term

To set the stage, we first discuss the tautological topological conservation law of lattice charges in an insulator and its dual response. The three-dimensional lattice volume form is

$$\text{volume(BZ)} = \mathbf{E}^1 \wedge \mathbf{E}^2 \wedge \mathbf{E}^3. \tag{4}$$

Related to this, the insulator has an integer number of filled electronic bands per unit cell (minus the positive background charge) and no free charges below the mobility gap [30]. The charge density (4) couples to the electric potential A_0 via the topological action [19,20]

$$S_{0D} = \frac{1}{(2\pi)^3} \int d^4x N_\omega \epsilon^{\mu\nu\lambda\rho} E_\mu^1 E_\nu^2 E_\lambda^3 A_\rho. \tag{5}$$

The invariant in terms of the (semiclassical) Green's function $G = G(\mathbf{p}, \omega)$ is

$$N_\omega(\mathbf{p}) = \frac{1}{2\pi i} \int_{-\infty}^{\infty} d\omega \mathrm{Tr} G \partial_\omega G^{-1} \tag{6}$$

and counts the number of occupied states in the BZ. The invariant $N_\omega \equiv N_\omega(\mathbf{p})$ can only change when the gap in the spectrum closes. This makes N_ω the simplest topological invariant possible. Note that the lattice vectors represented by the elasticity tetrads carry spatial indices only, therefore singling out the potential A_0. While the conservation of lattice volume is tautological to charge conservation below the (mobility) gap, and must be compensated by overall charge neutrality over the unit cell, the response (5) can be nontrivial when considered on the surface of a topological state with polarization [19], see below. This arises since the boundary response is dictated by overall conservation laws from nontrivial higher-dimensional bulk terms and often is anomalous as a purely lower-dimensional theory.

The response, thus understood, applies to insulators under elastic deformations, i.e., with coordinate dependence on the tetrads $\mathbf{E}^a$. The dual topological response corresponding to the lattice volume is the bulk theta term, corresponding to axion electrodynamics [47],

$$S = \frac{1}{32\pi^2} \int d^4x N_\theta(x,t) \epsilon^{\mu\nu\lambda\rho} F_{\mu\nu} F_{\lambda\rho} \tag{7}$$

coupling to zero-dimensional lattice points, i.e., the response of the original point charges. Here $F_{\mu\nu} = \partial_\mu A_\nu - \partial_\nu A_\mu$ is the electromagnetic tensor and

$$N_\theta(x,t) = \frac{1}{96\pi^2} \int_0^{2\pi} du \int_{\mathrm{BZ}} d\omega d^3\mathbf{p} \epsilon^{u\mu\nu\lambda\rho} \mathrm{Tr}\big[(G\partial_u G^{-1}) \times (G\partial_\mu G^{-1})(G\partial_\nu G^{-1})((G\partial_\lambda G^{-1})(G\partial_\rho G^{-1})\big] \tag{8}$$

with $\partial_\mu = (\partial_\omega, \partial_{\mathbf{p}})$ is the invariant corresponding to the whole frequency-momentum space, extended by the periodic adiabatic parameter u from dimensional reduction and related higher-dimensional anomalous theories defining the topological response; for more details see, e.g., Refs. [20,47–49]. The invariant is equal to the second Chern number and therefore reduces to an integral over the physical BZ. Time-reversal invariance and electric charge conservation suffice for nontrivial N_θ but are not necessary. With some other protecting symmetry K it reads

$$N_\theta' = \frac{1}{24\pi} \int_{\omega=0} d^3\mathbf{p} \mathrm{Tr}[\epsilon^{ijk} K (G^{-1}\partial_{p_i} G) \times (G^{-1}\partial_{p_j} G)(G^{-1}\partial_{p_k} G)],$$

where K is the operator representation of the symmetry transformation. Examples of such topological invariants are provided by the superfluid ^{3}He-B and the standard model of particle physics [50], when they are considered on the lattice. In other words, whereas in Eq. (6) $\mathbf{p}$ is fixed and the integral goes over the frequency, for the dual invariant the frequency is fixed and the integral goes over the momenta.

Combined with a protecting symmetry $N_\theta \to -N_\theta$, such as time-reversal or parity, and 2π periodicity due to the

quantized second Chern class, the theta term mod π implies the protected boundary modes on the surfaces of the insulator [47]. The invariant $N_\theta(x,t)$ is not quantized in general, however, and can be noninteger mod π [49,51], see also Ref. [52].

Next we discuss nontrivial topological crystalline responses that are tantamount to extra crystalline topological conservation laws, featuring the elasticity tetrads, in addition to electric charge conservation (gauge invariance). These also imply protected boundary modes in associated crystal directions. In summary, the crystalline responses and invariants require $U(1)$ electromagnetic and some crystalline translation symmetry only but remain well defined under point and space group symmetries, small elastic deformations, and open boundary conditions. Breaking the idealized crystalline translational symmetry in space under elastic deformations implies nonzero torsion in (3) associated with dislocations, see e.g. Ref. [53].

C. Anomalous QHE in 3D topological insulators

In particular, the elasticity tetrads are important in the field theory description of the intrinsic (without external magnetic field) quantum Hall effect in 3D topological and axion insulators [31,54–56]. The corresponding topological response contains the elasticity tetrad as a dynamical lattice gauge field combined with the electromagnetic gauge field with the Chern-Simons topological term [3,20,57–59]:

$$S[A,A,E]=\frac{1}{8\pi^2}\sum_{a=1}^{3}N_a\int d^4x\,E_\mu^{\ a}\epsilon^{\mu\nu\alpha\beta}A_\nu\partial_\alpha A_\beta. \quad (9)$$

The response resulting from this action is topologically nontrivial and the prefactor is expressed in terms of the topological charges in momentum space. This implies chiral fermion modes on the boundary, relevant for the 3D QHE along $N_a\mathbf{E}^a$ [see Eq. (12) below], as well as on dislocations [3]. For superconductors $\tilde{A}_\mu=A_\mu-\partial_\mu\phi$, where ϕ is the symmetry breaking phase mode, can enter [60] leading to chiral Majorana modes instead. The three independent integer quantized coefficients N_a are expressed in terms of integrals of the Green's functions in the energy-momentum space [57,58]:

$$N_a=\frac{1}{8\pi^2}\epsilon_{ijk}\int_{-\infty}^{\infty}d\omega\int_{\mathrm{BZ}}dS_a^i \times\mathrm{Tr}[(G\partial_\omega G^{-1})(G\partial_{p_j}G^{-1})(G\partial_{p_k}G^{-1})]. \quad (10)$$

Here the momentum integral is over the 2D torus—the 2D boundary $\mathbf{S}_a$ of the elementary cell of the 3D reciprocal lattice, see Fig. 1.

For a simple, say, orthorhombic lattice in Fig. 1, the topological charge describing the QHE in, say, the (x,y) plane is N_z. It is the integral in the (p_x,p_y) plane of the elementary cell of the reciprocal lattice at fixed p_z:

$$N_z(p_z)=\frac{1}{4\pi^2}\int_{-\infty}^{\infty}d\omega\int_{\mathrm{BZ}}dp^xdp^y \times\mathrm{Tr}[(G\partial_\omega G^{-1})(G\partial_{p_x}G^{-1})(G\partial_{p_y}G^{-1})]. \quad (11)$$

This integral in gapped crystalline insulators with AQHE does not depend on p_z, signaling the quantized response (9).

While in 2D crystals the topological invariant describes the quantization of the Hall conductance, the topological invariants N_a in 3D crystals describe the quantized response of the Hall conductivity to deformation [3]:

$$\frac{d\sigma_{ij}}{dE_k^{\ a}}=\frac{e^2}{2\pi h}\epsilon_{ijk}N_a. \quad (12)$$

The presence of the reciprocal lattice vector $E_k^{\ a}$ of dimension $1/[l]$ leads to the correct dimensions of the 3D conductivity, as expected.

D. Polarization and flat bands in 3D topological insulators

The three topological invariants N_a responsible for the 3D QHE are expressed in terms of integrals over three planar cross sections of the elementary cell of the three-dimensional reciprocal lattice, specified by perpendicular lattice directions. In three dimensions, there is another class of topological invariants represented by three invariants N^a in terms of line integrals along vectors of the reciprocal Bravais lattice that couple to perpendicular planes as in Fig. 1. Such a line forms a closed loop in the crystal that can, for example, accumulate a Zak phase π, see, e.g., Refs. [38,39] and Refs. [13,17].

The invariants N^a are related to a topological response that can be considered dual to the action (9), where one gauge field A_μ is substituted by the tetrad gauge field. This is given by the following topological term in the action

$$S[A,E,E]=\sum_{a=1}^{3}\frac{N^a}{8\pi^2}\epsilon_{abc}\int d^4xE_\mu^bE_\nu^c\epsilon^{\mu\nu\alpha\beta}\partial_\alpha A_\beta. \quad (13)$$

Likewise, since the term (13) is linear in the electric field $\mathcal{E}=\partial_t\mathbf{A}-\nabla A_0$, three invariants N^a $(a=1,2,3)$ characterize the topological polarization $\delta S[A,E,E]/\delta\mathcal{E}$ along three directions. It leads to the induced boundary charges from the bulk, in addition to modes bound on dislocations [19,20]. They are described by the action, assuming constant A_μ along boundary a for simplicity,

$$S_{\mathrm{bndry}}[A,E,E]=\frac{\Delta N^a}{8\pi^2}\epsilon_{abc}\int_{\mathrm{bndry}}d^3xE_\mu^bE_\nu^c\epsilon^{\mu\nu\alpha}A_\alpha. \quad (14)$$

This describes the surface polarization charge density coupling to A_0, and ΔN^a is the (integrated) bulk-boundary jump in N^a and the integral is perpendicular to the direction a. Similar to the case of Eq. (5), the static elasticity tetrads single out only the A_0 term. For superconductors, the combination $A_0-\partial_t\phi$ can enter [60], with Majorana modes from polarization [18]. Moreover, the boundary theory can be anomalous when considered without the associated bulk [19,30].

From the comparison of the polarization to the Zak phase, see, e.g., Refs. [13,17,18] for insulators and superconductors and Refs. [38,39] for gapless systems, we conclude that in some cases the invariants N^a can be written simply in terms of an effective Hamiltonian $H(\mathbf{p})=1/G(\mathbf{p},\omega=0)$, which is the inverse of the Green's function at zero frequency. The polarization invariant can be more generally linked to the semiclassical expansion for the momentum space invariants discussed in Ref. [20]. Here we assume that the insulator is PT symmetric, i.e., obeys the combination of time reversal and space inversion symmetries, and thus the PT

operation anticommutes with the Hamiltonian. It is important that the operator PT is local in momentum space (see also Refs. [61,62]), so that we can write the invariant in terms of an effective Hamiltonian. In particular, for an orthorhombic lattice the invariant is

$$N^z(p_x, p_y) = \frac{1}{2\pi i}\mathrm{Tr}\left[PT \oint dp_z H^{-1}\partial_{p_z} H\right]. \quad (15)$$

Similar to the invariant $N_z(p_z)$, which does not depend on p_z in insulators, the invariant $N^z(p_x, p_y)$ does not depend on the transverse momenta $\mathbf{p}_\perp$ in the gapped systems (insulators or superconductors).

In noninteracting PT-symmetric insulators [17] and superconductors [18] these invariants determine the Berry phase change along the loop (the Zak phase), which is $2\pi N^a$. In nodal line semimetals the nonzero Zak phase produces zero-energy surface states, which form a flat band [38,39]. In gapped crystalline insulators, where the invariants do not depend on $p_\perp$, the flat band occupies the whole Brillouin zone on the corresponding boundaries of the sample. Note that the exact flatness of these surface bands relies on a chiral symmetry often present especially in nodal line superconductors [42] but also in approximative descriptions of nodal line semimetals [38]. This symmetry is not necessary for the stability of the nodal lines [41,63], but in its absence the surface states become "drumhead" states with some dispersion. The same is expected for the approximately flat bands of the crystalline insulator [17].

E. Dual invariants and quantized electric polarization response

To gain insight to the dual responses, including the polarization, let us consider for simplicity an orthorhombic crystal with an electric field along z. From Fig. 1, the invariants N^a can be considered as geometric duals to the three invariants N_a in the crystalline lattice. While the invariant N_3 is an integral over the surface formed by two vectors, $\mathbf{E}^1 \wedge \mathbf{E}^2$, the invariant N^3 is an integral on the path along the vector $\mathbf{E}^3$. They respectively couple to the tetrads $\mathbf{E}^3$ and $\mathbf{E}^1 \wedge \mathbf{E}^2$ in the response.

We now focus explicitly on the polarization. Then the appropriate part of the action contains the invariant N^3:

$$S[A, E, E] = \frac{N^3}{4\pi^2}\int d^4x(\mathbf{E}^1 \times \mathbf{E}^2)\cdot\mathcal{E} = \frac{N^3}{4\pi^2}\int d^4x\, \mathbf{S}^{12}\cdot\mathcal{E}, \quad (16)$$

where $\mathbf{S}^{12}$ is the area of the 2D BZ in the plane perpendicular to the normal of the considered boundary.

Electric polarization is determined as the response of the action to the electric field $\mathcal{E}$ in the limit of infinitesimal electric field, $\mathcal{E} \to 0$. From Eq. (16) it looks that for the topological insulator with $N^a \neq 0$, the polarization is nonzero in zero electric field, which is, however, forbidden by parity symmetry or by the PT invariance. In fact, it is forbidden for the infinite sample, while in the presence of boundaries this is possible, since boundaries violate parity symmetry, similar to the time-reversal symmetry and surface modes with theta term. In the presence of two boundaries there are two degenerate ground states with opposite polarization. In one state the positive electric charges are concentrated on the upper boundary (with electric charge $+|e|/2$ per one state in the flat band), and the negative charges are on the lower boundary. In the other degenerate state the polarization is opposite. The first state is obtained as a response to the electric field $\mathcal{E}_z \to +0$, while the second state is obtained in the limit $\mathcal{E}_z \to -0$. This means that the integer topological polarization can be considered as the difference in polarization, when the electric field changes sign.

Recent calculations of the topological polarization in nodal loop semimetals have been done in Ref. [9]. We consider this for crystalline topological insulators where the response is quantized in terms of the elasticity tetrads. Similar to the response of the QHE to deformations in Eq. (12), which is quantized in crystalline topological insulators in terms of invariants N_a, the response of the topological polarization to strain is quantized in terms of the invariants N^a. From Eq. (16) it follows that the quantized response corresponding to the polarization $P^i = \delta S/\delta\mathcal{E}_i|_{\mathcal{E}=0}$ is the deformation of the cross sectional area in the reciprocal lattice:

$$\frac{dP^i}{dS^{ab,k}} = \frac{1}{4\pi^2}\delta^i_k\epsilon_{abc}N^c. \quad (17)$$

For the simple orthorhombic crystal and for polarization along z this becomes

$$\frac{dP^z}{dS^{12}} = \frac{1}{4\pi^2}N^3. \quad (18)$$

The quantized variation of the polarization with respect to deformation is an example of a well defined "differential" polarization [6,8]. Note that the polarization itself is not quantized, depending on (the surface spanned by) the reciprocal lattice vectors, but its derivative with respect to deformation in Eq. (17) is quantized.

III. POLARIZATION AND FLAT BAND IN A NUMERICAL MODEL

In 3D topological insulators, the same invariant N^a hence implies both the flat band on the surface of the material and the topological polarization in the bulk response. In general terms, this is an example of bulk-boundary correspondence or anomaly inflow from the bulk to the boundary, as discussed above.

More concretely, this follows since each $\mathbf{p}_\perp$ in the system represents a $1+1d$ topological insulator, and thus for each $\mathbf{p}_\perp$ there should be a zero energy state on the boundary. Thus for the topological insulators with nonzero N^c the flat band exists on the surface for all $\mathbf{p}_\perp$. This is distinct from nodal line semimetals, where the region of the surface flat band is bounded by the projection of the nodal line to the boundary. The topological insulator phase can be obtained when the Dirac loop is moved to the boundary of the BZ.

This can be verified using an extension of the model $H = \begin{pmatrix} & f \\ f^* & \end{pmatrix}$ in Ref. [38] with $f = \sin p_x + i\sin p_y - te^{-ip_z}$, i.e., the Hamiltonian in the limit of infinite number of layers is

$$H = \sigma_x(\sin p_x - t\cos p_z) + \sigma_y(\sin p_y - t\sin p_z). \quad (19)$$

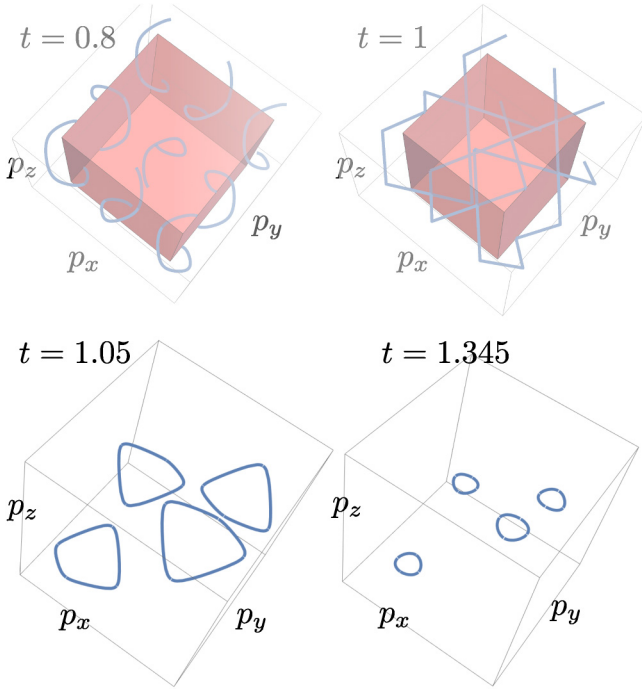

FIG. 2. Nodal lines for different parameters t. In top figures showing the spiral lines up to $t = 1$, the first Brillouin zone is shown as a box. In bottom figures, only the first Brillouin zone is plotted.

For low enough t, the nodal line can be found at the momenta p_x, p_y, p_z that simultaneously nullify the coefficients of $\sigma_{x,y}$. This model has three different phases depending on the value of the coefficient t as illustrated in Figs. 2 and 3. For $t < 1$, the first Brillouin zone contains four spiral lines: one inside it and others going through the Brillouin zone boundaries. In this case there are surface flat bands at the projection of the spirals to the surfaces. At $t = 1$ these lines touch and cut each other to form closed nodal line loops when $1 < t < \sqrt{2}$.

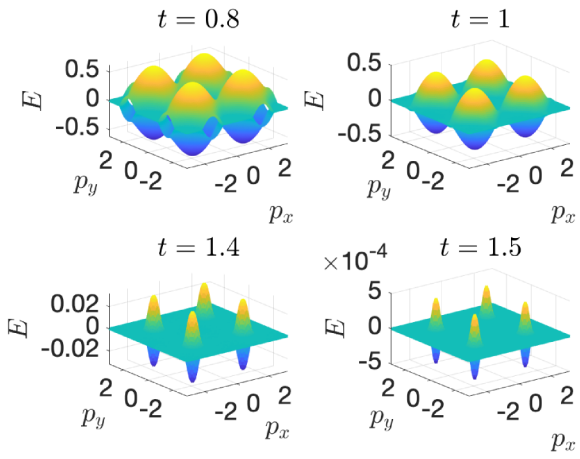

FIG. 3. Two lowest-energy eigenstates near $E = 0$, showing how for $t < \sqrt{2}$ the flat bands extend through part of the first Brillouin zone, and for $t > \sqrt{2}$ across the entire BZ. In the figure with $t = 1.5$, the shown finite energy is associated to the finite number of layers in the simulation (note the energy scale that is lower than in other plots). All plots are computed with $N = 100$ layers.

The projection of these loops to the surface still marks the boundaries of the surface flat bands. Finally, for $t = \sqrt{2}$ the loops shrink into four nodal points and vanish for $t > \sqrt{2}$ in which case the system forms a topological insulator. In this case the flat band extends throughout the 2D Brillouin zone of the transverse momenta. This behavior is qualitatively similar to that found for the slightly more complicated model of rhombohedrally stacked honeycomb lattice [63].

The topological invariant (15) is in Eq. (5) of Ref. [38], where the PT operator is played by σ_z. In terms of the unit vector of Pauli matrices in the Green's function $\hat{\mathbf{g}}(\mathbf{p}, \omega) \equiv \frac{\mathbf{G}}{|\mathbf{G}|}$ the invariant is in Eq. (8) of Ref. [38]:

$$N^3(\mathbf{p}_\perp) = \frac{1}{4\pi} \oint_{-\pi/a}^{\pi/a} dp_z \int_{-\infty}^{\infty} d\omega \hat{\mathbf{g}} \cdot \left(\frac{\partial \hat{\mathbf{g}}}{\partial p_z} \times \frac{\partial \hat{\mathbf{g}}}{\partial \omega} \right). \quad (20)$$

In the case of the Hamiltonian in Eq. (19), in the nodal line phase corresponding to $t < \sqrt{2}$, $N^3(\mathbf{p}_\perp)$ is nonzero inside the projection of the nodal lines to the 2D space $\mathbf{p}_\perp$ and zero outside it. On the other hand, in the topological insulator phase with $t > \sqrt{2}$, $N^3(\mathbf{p}) = 1$ for all transverse momenta.

For a finite number of layers the Hamiltonian matrix is

$$H_{ij} = (\sigma_x \sin p_x + \sigma_y \sin p_y)\delta_{ij} - t(\sigma^+ \delta_{i,j+1} + \sigma^- \delta_{i,j-1}). \quad (21)$$

This can be used to compute the spectrum shown in Fig. 3. Moreover, using the (spinor) eigenstates $\phi_n(j, p_x, p_y)$ of the finite-system Hamiltonian corresponding to eigenenergy ϵ_n, we also get the charge density at layer j

$$\rho_j = \rho_0 - e \sum_n \int_{BZ} \frac{d^{(2)}p}{(2\pi)^2} f(\epsilon_n) \phi_n(j, p_x, p_y)^\dagger \phi_n(j, p_x, p_y). \quad (22)$$

Here the integral goes over the 2D Brillouin zone of size S^{12} of the transverse momenta, $f(\epsilon)$ is the Fermi distribution, and $\rho_0 = eS^{12}/(4\pi^2)$ ensures a charge neutral situation at zero chemical potential. We calculate everything at zero temperature.

In a given electric field, the polarization can be computed as

$$P^z = \frac{1}{d} \sum_{j=1}^{N} \rho_j (x_j - d/2), \quad (23)$$

where $x_j = ja$, $d = Na$ is the thickness of the system, N is the number of layers, and a is the lattice constant (layer separation). We calculate this polarization in the case of an applied electric field similarly to in Ref. [9] (see Appendix for details) [64]. We concentrate on the case of negligible screening, i.e., disregard the backaction of the charge density to the electric field. This corresponds to the limit $\alpha \to 0$ in Ref. [9]. In other words, we consider a linearly growing potential describing the effect of the field. The results are shown in Fig. 4. Due to the presence of the flat bands, a small electric field leads to a charge density that is antisymmetric with respect to the center of the system (the average charge hence vanishes), i.e., a nonzero charge polarization. This polarization jumps rather abruptly as a function of the sign of the electric field. The size of the jump is integer

$$P^z(\mathcal{E}_z > 0) - P^z(\mathcal{E}_z < 0) = e\frac{\Omega_{\mathrm{FB}}}{4\pi^2}, \quad (24)$$

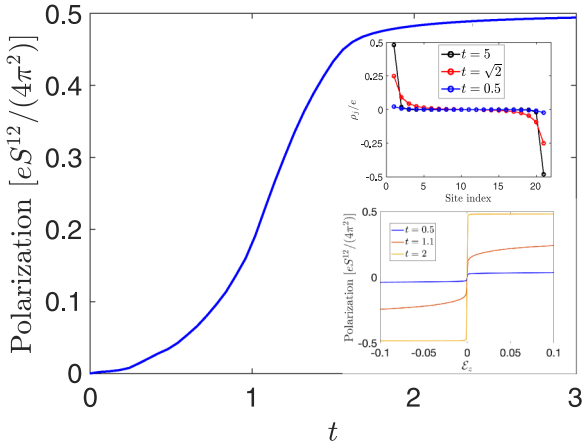

FIG. 4. Polarization as a function of the hopping parameter t driving two Lifshitz transitions from two types of nodal line semimetals at $t < 1$ and $1 < t < \sqrt{2}$ to a topological insulator phase at $t > \sqrt{2}$. Upper inset: charge density for a few parameter values indicated in the legend. Lower inset: polarization as a function of the electric field $\mathcal{E}_z$. If not specified otherwise, the figures are calculated with $N = 21$ layers and with electric field $\mathcal{E}_z = 0.1$.

where $\Omega_{\rm FB}$ is the area of the flat band in momentum space. In the topological insulator phase $t > \sqrt{2}$ the size of the flat band becomes equal to the size of the 2D Brillouin zone, $\Omega_{\rm FB} = S^{12}$, and hence we get the result of Eq. (18). This is numerically identified in Fig. 4 where the slight deviation of the polarization from 0.5 after the transition to the polarized insulator is a finite-size effect.

Note that the model described here contains a chiral symmetry: H anticommutes with the PT symmetry operator σ_z. Such chiral symmetries are typically not encountered in crystal lattices, but they may be approximate symmetries in their model Hamiltonians (for the case of rhombohedral graphite, see Ref. [65]). Chiral symmetry breaking terms do not destroy the surface states, but in their presence the surface states become drumhead states with a nonzero bandwidth $\delta\epsilon$ (see Appendix B). In this case the polarization no longer contains an abrupt jump as a function of the field, but the jump has a finite width. Nevertheless, the size of the jump remains the same as in Eq. (24). Note that the quantized jump requires that the bulk states do not contribute to the polarization response even at the finite electric field required to see it. This then remains well defined in the topological insulator state provided the chiral symmetry breaking terms are small compared to the bulk gap.

IV. CONCLUSION AND OUTLOOK

We discuss the topological responses in three-dimensional crystalline insulators (and superconductors) in terms of dual pairs of invariants and the elasticity tetrads. We focus on the topological polarization response and the associated flat bands at the boundaries. We show the explicit momentum space invariant linking the bulk and boundary. We also demonstrate the formation of the topological polarization in the case of an example Hamiltonian specified in Eqs. (19) and (21). This polarization response and modes are distinct from, e.g., the bulk theta term in time reversal invariant topological insulators, in that they are protected only by the associated (weak) crystalline symmetries.

We also discuss the relation of polarization to the other possible invariants in three dimensions and the structure of the responses in terms of the elasticity tetrads. The elasticity tetrads themselves are defined in terms of the Bravais lattice, taken here to be orthorhombic for simplicity. The dependence of the crystalline response, such as polarization, on the chosen unit cell requires some care [15]. The formal requirement of our continuum theory is that the chosen unit cell should be small compared to the gradients of the external fields. Thus the unit cell is averaged over in the response and the small gradients probe what was called "inter-unit-cell entanglement" in Refs. [13,15,19]. At higher gradients, the response would be of identical form but contain also polarization over the unit-cell geometry. For the invariants, on the other hand, sublattice geometry is of course very essential, see, e.g., the numerical model (19) and the recent paper [66].

In more detail, the one-dimensional topological invariant (the Zak phase) in Eqs. (15) and (20) describes two related phenomena: the topological response of polarization to the strain and the surface flat band. This demonstrates that the bulk topological polarization implies the filling of the zero energy surface states and vice versa, constituting an example of bulk-boundary correspondence and the associated anomaly inflow. Notably, the bulk polarization response is a total derivative in the absence of boundaries and dislocations. Moreover, one can show that explicit bulk and boundary currents in the polarized insulators require (adiabatic) time dependence in the polarization invariants, see Eq. (13). Nevertheless, likely the almost flat surface states can be made metallic or delocalized, e.g., if the surface chemical potential is changed or by nontrivial topology transverse to the polarization. We leave the detailed study of this and properties encompassing several or all bulk crystalline invariants for future.

We note that the different crystalline invariants in the responses discussed are integer periodic by translational lattice and gauge symmetry. For example, the polarization response is proportional to the topological first Chern number $\int \frac{F}{2\pi}$ in the lattice direction a, which is an integer over closed manifolds, times a spatial volume integral counting the number of lattice points in the perpendicular direction. Similar interpretation holds for the other crystalline invariants [20,44,46]. The conclusion is that the topological polarization N^a, or the other crystalline responses and invariants, are defined mod integers by translational and U(1) symmetries, as expected [44]. Overall, the bulk state remains sensitive to the invariant, lattice geometry, and boundary conditions.

Like in time-reversal invariant insulators, the invariants can be exactly quantized in the presence of twofold symmetries, such as inversion. More complicated crystalline symmetries lead to other quantized values [11,12,67]. Under perturbations breaking the symmetries, the invariants remain quantized in some finite region and the mixing of the protected modes with generic bulk states remains suppressed by the smallness of the perturbation.

Using the simple numerical model in Sec. III with polarization, the protecting symmetry is the chiral PT symmetry,

where the additional time-reversal symmetry T fixes the surface modes at exactly zero energy, rendering them flat bands, see also Appendix B. However, the latter is not strictly required since the electric field is T even, in analogy to protecting symmetry of the adjacent nodal semimetal phase [38–41]. We explicitly verified that the response of the polarization to the properly defined deformations is quantized, see Eq. (17), and that the corresponding surface flat band is present throughout the whole BZ. This is distinct from the nodal line semimetals, where there is also a flat band, but where this flat band occupies only part of the surface BZ. As a result there is no bulk quantization. The surface polarization and theory become anomalous in terms of a mere two-dimensional description, and they have to be discussed in the context of the bulk-boundary correspondence, including the gapless fermions. However, the polarization difference and derivative with respect to the deformation becomes quantized precisely when the nodal loop moves to the boundaries of the BZ and annihilates, forming a gapped topological insulator.

This situation is very similar to that in the AQHE, implying the presence of protected chiral edge modes. In 3D topological crystalline insulators it is the derivative of the Hall conductivity which is quantized [20] and well defined. In the Weyl semimetals such quantization is absent, implying the chiral anomaly from the gapless fermions, but is restored when the Weyl nodes move to the boundaries of the BZ and annihilate forming a topological insulator, see, e.g., Refs. [20,68,69]. More generally, the connection and evolution of the gapped crystalline responses and invariants with elasticity tetrads to unquantized anomalies in adjacent semimetal phases remains an interesting problem [70–74] as well as topological elasticity [35,36,44].

Systems with flat bands are strongly susceptible to interaction induced broken symmetry phases such as superconductivity [40]. There, the (mean field) transition temperature T_c is proportional to the volume of the flat band, if the flat band is formed in the bulk [75], or to the area of the flat band if it is formed on the surface of the sample [39]. Topological insulators have a larger area of the flat band compared with the flat bands on the surface of nodal line semimetals, and thus they may have a higher T_c. This is in contrast, for example, to the Moiré superlattice in magic angle twisted bilayer graphene, where the flat band extends across the first Brillouin zone of the superlattice [76–78]. At the magic angle the superlattice unit cell contains a large number $N \sim 10^4$ of atoms, implying a rather small flat band with area $\sim 1/(Na^2)$, where a is the graphene lattice constant. Nevertheless, the recent measurements [79,80] indicate superconductivity with a T_c around a few K. This means that topological insulators with much larger flat bands may be included in the competition whose final goal is room-temperature superconductivity. Other current participants in the race are hydrogen-rich materials, such as H_3S, LaH_{10}, Li_2MgH_{16}, YH_6, etc. [81–85]. In these systems, the large transition temperature results from the large vibrations of light hydrogens, which increase the electron-phonon coupling. The contributions of flat band and vibrations would ideally be combined. The manipulation and control of acoustic vibrations in insulators (which represent massive and massless "gravitons" in terms of the lattice metric and elasticity tetrads with elastic energy, respectively [28]) is not an easy task. But if the surface flat band of the insulator is in contact with hydrogen-rich material, then the electron-phonon interaction between phonons in hydrides and electrons in the flat band may conspire in increasing T_c even further.

Lastly, we note that a phase with periodic stringlike order parameter in spin chains was recently found to lead to topological flat bands of Majoranas [86]. This is probably related to the polarization in the crystalline superconductors. On the other hand, another recent flat-band work describing lattices of fermions with random interactions [87,88] is rather related to the Khodel-Shaginyan Fermi condensate [75].

ACKNOWLEDGMENTS

This work has been supported by the European Research Council (ERC) under the European Union's Horizon 2020 research and innovation programme (Grant Agreement No. 694248) and the Academy of Finland (project No. 317118).

APPENDIX A: DETAILS OF THE NUMERICS

Figure 2 is produced by a parametric plot exhibiting the simultaneous solutions to the equations

$$\sin(p_x) = t\,\sin(p_z); \sin(p_y) = t\,\cos(p_z).$$

Figure 3 is obtained by constructing the $2N \times 2N$ matrix corresponding to Eq. (21). The plotted quantity corresponds to the two center eigenvalues, which are the lowest-energy eigenstates at $\mu = 0$ for the particle-hole symmetric Hamiltonian [64].

Figure 4 finds the eigenstates of the Hamiltonian $H_{ij} - \mu_j \delta_{ij}$ with a layer dependent potential μ_j. To mimic an electric field in the direction perpendicular to the layers, we follow Ref. [9] and choose

$$\mu_j = \mathcal{E}_z(j - N/2).$$

Using the resulting eigenstates and -energies, we then calculate the charge density Eq. (22) and polarization Eq. (23). Note that this approach neglects the changes into μ_j that would come from solving the Poisson equation. It hence corresponds to the limit $\kappa \to \infty$ or $\alpha \to 0$ in Ref. [9]. The case of a finite κ would lead to a possibility of broadening of the polarization step but would not affect the size of the step. As shown below, a similar broadening would be produced by weak chiral symmetry breaking.

APPENDIX B: EFFECT OF CHIRAL SYMMETRY BREAKING

We study the effect of chiral symmetry breaking on the polarization jump by adding a term

$$g \sin p_x \sin p_y \sigma_0 (\delta_{i,j+1} + \delta_{i,j-1}) \tag{B1}$$

to the Hamiltonian (21). This does not anticommute with the PT symmetry operator σ_z. As a result, it lifts the flat-band degeneracy of the surface states and leads to drumhead-type dispersion shown in Fig. 5. The effect on the polarization jump is plotted in Fig. 6. In this case the jump ceases to be abrupt, but the overall size of the jump is unaltered, and the unit polarization is recovered after the drumhead states are filled.

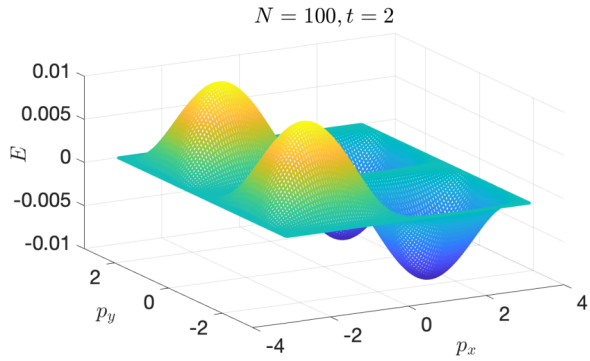

FIG. 5. Drumhead dispersion in the topological insulator state with $t = 2$ in the presence of a chiral symmetry breaking term with $g = 0.01$. The bandwidth produced by this symmetry breaking term is still small compared to the insulator gap of $t - \sqrt{2}$.

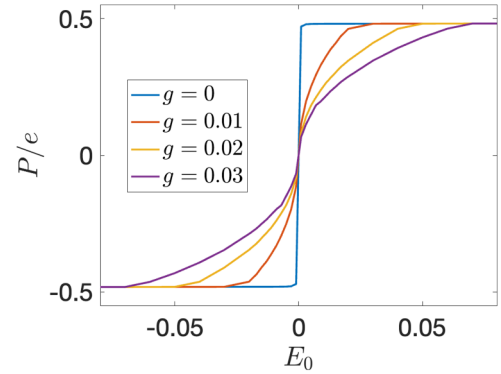

FIG. 6. Polarization jump in the presence of chiral symmetry breaking. The abrupt jump becomes smoother, but the amplitude of the jump remains quantized.

[1] M. Z. Hasan and C. L. Kane, Colloquium: Topological insulators, Rev. Mod. Phys. **82**, 3045 (2010).

[2] The discussion in this paper is for spinless fermions. In other words, we do not concentrate on the distinction between time-reversal symmetry breaking quantum Hall effect and the spin quantum Hall effect relevant in the presence of time reversal symmetry.

[3] B. I. Halperin, Possible states for a three-dimensional electron gas in a strong magnetic field, Jpn. J. Appl. Phys. **26**, 1913 (1987).

[4] R. Roy, Topological phases and the quantum spin Hall effect in three dimensions, Phys. Rev. B **79**, 195322 (2009).

[5] R. D. King-Smith and D. Vanderbilt, Theory of polarization of crystalline solids, Phys. Rev. B **47**, 1651 (1993).

[6] R. Resta, Macroscopic polarization in crystalline dielectrics: the geometric phase approach, Rev. Mod. Phys. **66**, 899 (1994).

[7] G. Ortiz and R. M. Martin, Macroscopic polarization as a geometric quantum phase: Many-body formulation, Phys. Rev. B **49**, 14202 (1994).

[8] R. Resta, Electrical polarization and orbital magnetization: the modern theories, J. Phys.: Condens. Matter **22**, 123201 (2010).

[9] Y. Ominato, A. Yamakage, and K. Nomura, Electric polarization in magnetic topological nodal semimetal thin films, Condensed Matter **3**, 43 (2018).

[10] N. P. Armitage and L. Wu, On the matter of topological insulators as magnetoelectrics, SciPost Phys. **6**, 046 (2019).

[11] A. Alexandradinata, X. Dai, and B. A. Bernevig, Wilson-loop characterization of inversion-symmetric topological insulators, Phys. Rev. B **89**, 155114 (2014).

[12] A. Alexandradinata and B. A. Bernevig, Berry-phase description of topological crystalline insulators, Phys. Rev. B **93**, 205104 (2016).

[13] J.-W. Rhim, J. Behrends, and J. H. Bardarson, Bulk-boundary correspondence from the intercellular Zak phase, Phys. Rev. B **95**, 035421 (2017).

[14] G. van Miert and C. Ortix, Excess charges as a probe of one-dimensional topological crystalline insulating phases, Phys. Rev. B **96**, 235130 (2017).

[15] H. Watanabe and M. Oshikawa, Inequivalent Berry Phases for the Bulk Polarization, Phys. Rev. X **8**, 021065 (2018).

[16] A. S. Sergeev, Geometry of projected connections, Zak phase, and electric polarization, Phys. Rev. B **98**, 161101(R) (2018).

[17] Y. Aihara, M. Hirayama, and S. Murakami, Anomalous dielectric response in insulators with the π Zak phase, Phys. Rev. Research **2**, 033224 (2020).

[18] J. C. Budich and E. Ardonne, Equivalent topological invariants for one-dimensional Majorana wires in symmetry class D, Phys. Rev. B **88**, 075419 (2013).

[19] X.-Y. Song, Y.-C. He, A. Vishwanath, and C. Wang, Electric polarization as a nonquantized topological response and boundary Luttinger theorem, Phys. Rev. Research **3**, 023011 (2021).

[20] J. Nissinen and G. E. Volovik, Elasticity tetrads, mixed axial-gravitational anomalies, and (3+1)-d quantum Hall effect, Phys. Rev. Research **1**, 023007 (2019).

[21] I. E. Dzyaloshinskii and G. E. Volovik, Poisson brackets in condensed matter physics, Ann. Phys. **125**, 67 (1980).

[22] J. Nissinen and G. E. Volovik, Tetrads in solids: from elasticity theory to topological quantum Hall systems and Weyl fermions, J. Exp. Theor. Phys. **127**, 948 (2018).

[23] G. E. Volovik, Dimensionless physics, ZhETF **159**, 815 (2021) [JETP **132**, 727 (2021)].

[24] C. Wetterich, Spontaneous Symmetry Breaking Origin for the Difference between Time and Space, Phys. Rev. Lett. **94**, 011602 (2005).

[25] D. Diakonov, Towards lattice-regularized quantum gravity, arXiv:1109.0091.

[26] A. A. Vladimirov and D. Diakonov, Phase transitions in spinor quantum gravity on a lattice, Phys. Rev. D **86**, 104019 (2012).

[27] Y. N. Obukhov and F. W. Hehl, Extended Einstein–Cartan theory à la Diakonov: the field equations, Phys. Lett. B **713**, 321 (2012).

[28] C. Wetterich, Geometry and symmetries in lattice spinor gravity, Ann. Phys. **327**, 2184 (2012).

[29] A. A. Vladimirov and D. Diakonov, Diffeomorphism-invariant lattice actions, Phys. Part. Nuclei **45**, 800 (2014).

[30] M. Oshikawa, Commensurability, Excitation Gap, and Topology in Quantum Many-Particle Systems on a Periodic Lattice, Phys. Rev. Lett. **84**, 1535 (2000).

[31] Here the invariant N_a describes a system with a broken time reversal symmetry, in which case the response is an anomalous quantum Hall effect. The spin quantum Hall effect without time reversal breaking can be obtained by a simple modification of the invariant to include the PT symmetry operator inside the trace.

[32] H. Song, S.-J. Huang, L. Fu, and M. Hermele, Topological Phases Protected by Point Group Symmetry, Phys. Rev. X **7**, 011020 (2017).

[33] S.-J. Huang, H. Song, Y.-P. Huang, and M. Hermele, Building crystalline topological phases from lower-dimensional states, Phys. Rev. B **96**, 205106 (2017).

[34] R. Thorngren and D. V. Else, Gauging Spatial Symmetries and the Classification of Topological Crystalline Phases, Phys. Rev. X **8**, 011040 (2018).

[35] A. Gromov, Chiral Topological Elasticity and Fracton Order, Phys. Rev. Lett. **122**, 076403 (2019).

[36] D. V. Else, S.-J. Huang, A. Prem, and A. Gromov, Quantum many-body topology of quasicrystals, arXiv:2103.13393.

[37] L. Fu, C. L. Kane, and E. J. Mele, Topological Insulators in Three Dimensions, Phys. Rev. Lett. **98**, 106803 (2007).

[38] T. T. Heikkilä and G. E. Volovik, Dimensional crossover in topological matter: Evolution of the multiple Dirac point in the layered system to the flat band on the surface, JETP Lett. **93**, 59 (2011).

[39] T. T. Heikkilä, N. B. Kopnin, and G. E. Volovik, Flat bands in topological media, JETP Lett. **94**, 233 (2011).

[40] N. B. Kopnin, T. T. Heikkilä, and G. E. Volovik, High-temperature surface superconductivity in topological flat-band systems, Phys. Rev. B **83**, 220503(R) (2011).

[41] A. A. Burkov, M. D. Hook, and L. Balents, Topological nodal semimetals, Phys. Rev. B **84**, 235126 (2011).

[42] A. P. Schnyder and S. Ryu, Topological phases and surface flat bands in superconductors without inversion symmetry, Phys. Rev. B **84**, 060504(R) (2011).

[43] V. B. Eltsov, T. Kamppinen, J. Rysti, and G. E. Volovik, Topological nodal line in superfluid ^{3}He and the Anderson theorem, arXiv:1908.01645.

[44] J. Nissinen, Field theory of higher-order topological crystalline response, generalized global symmetries and elasticity tetrads, arXiv:2009.14184.

[45] T. I. Tuegel, V. Chua, and T. L. Hughes, Embedded topological insulators, Phys. Rev. B **100**, 115126 (2019).

[46] O. Dubinkin, A. Rasmussen, and T. L. Hughes, Higher-form gauge symmetries in multipole topological phases, Ann. Phys. **422**, 168297 (2020).

[47] X.-L. Qi, T. L. Hughes, and S.-C. Zhang, Topological field theory of time-reversal invariant insulators, Phys. Rev. B **78**, 195424 (2008).

[48] G. E. Volovik, An analog of the quantum Hall effect in a superfluid ^{3}He film, ZhETF **94**, 123 (1988) [Sov. Phys. JETP **67**, 1804 (1988)].

[49] J. I. Väyrynen and G. E. Volovik, Soft topological objects in topological media, JETP Lett. **93**, 344 (2011).

[50] G. E. Volovik, Topological invariants for standard model: From semi-metal to topological insulator, JETP Lett. **91**, 55 (2010).

[51] M. Mulligan and F. J. Burnell, Topological insulators avoid the parity anomaly, Phys. Rev. B **88**, 085104 (2013).

[52] M. Kurkov and D. Vassilevich, How Many Surface Modes does one See on the Boundary of a Dirac Material?, Phys. Rev. Lett. **124**, 176802 (2020).

[53] A. J. Beekman, J. Nissinen, K. Wu, and J. Zaanen, Dual gauge field theory of quantum liquid crystals in three dimensions, Phys. Rev. B **96**, 165115 (2017).

[54] C. Wang, L. Gioia, and A. A. Burkov, Fractional Quantum Hall Effect in Weyl Semimetals, Phys. Rev. Lett. **124**, 096603 (2020).

[55] M. Thakurathi and A. A. Burkov, Theory of the fractional quantum hall effect in weyl semimetals, Phys. Rev. B **101**, 235168 (2020).

[56] D. Sehayek, M. Thakurathi, and A. A. Burkov, Charge density waves in weyl semimetals, Phys. Rev. B **102**, 115159 (2020).

[57] T. Matsuyama, Quantization of conductivity induced by topological structure of energy-momentum space in generalized QED3, Prog. Theor. Phys. **77**, 711 (1987).

[58] K. Ishikawa and T. Matsuyama, Magnetic field induced multicomponent QED3 and quantum Hall effect, Z. Phys. C **33**, 41 (1986).

[59] M. F. L. Golterman, K. Jansen, and D. B. Kaplan, Chern-simons currents and chiral fermions on the lattice, Phys. Lett. B **301**, 219 (1993).

[60] M. Stone and R. Roy, Edge modes, edge currents, and gauge invariance in $px + ipy$ superfluids and superconductors, Phys. Rev. B **69**, 184511 (2004).

[61] Y. X. Zhao, A. P. Schnyder, and Z. D. Wang, Unified Theory of PT and CP Invariant Topological Metals and Nodal Superconductors, Phys. Rev. Lett. **116**, 156402 (2016).

[62] C. K. Chiu, Y. H. Chan, and A. P. Schnyder, Quantized Berry phase and surface states under reflection symmetry or space-time inversion symmetry, arXiv:1810.04094.

[63] T. Hyart, R. Ojajärvi, and T. T. Heikkilä, Two topologically distinct Dirac-line semimetal phases and topological phase transitions in rhombohedrally stacked honeycomb lattices, J. Low Temp. Phys. **191**, 35 (2018).

[64] The codes needed to reproduce Figs. 3–6 can be found at https://gitlab.jyu.fi/jyucmt/topological-polarization.

[65] N. B. Kopnin, M. Ijäs, A. Harju, and T. T. Heikkilä, High-temperature surface superconductivity in rhombohedral graphite, Phys. Rev. B **87**, 140503 (2013).

[66] S. H. Simon and M. S. Rudner, Contrasting lattice geometry dependent versus independent quantities: Ramifications for Berry curvature, energy gaps, and dynamics, Phys. Rev. B **102**, 165148 (2020).

[67] M. Di Liberto, N. Goldman, and G. Palumbo, Non-Abelian Bloch oscillations in higher-order topological insulators, Nat. Commun. **11**, 5942 (2020).

[68] A. A. Zyuzin and A. A. Burkov, Topological response in Weyl semimetals and the chiral anomaly, Phys. Rev. B **86**, 115133 (2012).

[69] S. T. Ramamurthy and T. L. Hughes, Patterns of electromagnetic response in topological semimetals, Phys. Rev. B **92**, 085105 (2015).

[70] J. Nissinen, Emergent Spacetime and Gravitational Nieh-Yan Anomaly in Chiral $p + ip$ Weyl Superfluids and Superconductors, Phys. Rev. Lett. **124**, 117002 (2020).

[71] J. Nissinen and G. E. Volovik, On thermal Nieh-Yan anomaly in topological Weyl materials, JETP Lett. **110**, 789 (2019).

[72] J. Nissinen and G. E. Volovik, Thermal Nieh-Yan anomaly in Weyl superfluids, Phys. Rev. Research **2**, 033269 (2020).

[73] S. Laurila and J. Nissinen, Torsional Landau levels and geometric anomalies in condensed matter Weyl systems, Phys. Rev. B **102**, 235163 (2020).

[74] L. Gioia, C. Wang, and A. A. Burkov, Unquantized anomalies in topological semimetals, arXiv:2103.09841.

[75] V. R. Khodel and V. A. Shaginyan, Superfluidity in system with fermion condensate, JETP Lett. **51**, 553 (1990).

[76] E. S. Morell, J. D. Correa, P. Vargas, M. Pacheco, and Z. Barticevic, Flat bands in slightly twisted bilayer graphene: Tight-binding calculations, Phys. Rev. B **82**, 121407(R) (2010).

[77] R. Bistritzer and A. H. MacDonald, Moire bands in twisted double-layer graphene, Proc. Natl. Acad. Sci. **108**, 12233 (2011).

[78] T. J. Peltonen, R. Ojajärvi, and T. T. Heikkilä, Mean-field theory for superconductivity in twisted bilayer graphene, Phys. Rev. B **98**, 220504 (2018).

[79] Y. Cao, V. Fatemi, S. Fang, K. Watanabe, T. Taniguchi, E. Kaxiras, and P. Jarillo-Herrero, Unconventional superconductivity in magic-angle graphene superlattices, Nature (London) **556**, 43 (2018).

[80] M. Yankowitz, S. Chen, H. Polshyn, Y. Zhang, K. Watanabe, T. Taniguchi, D. Graf, A. F. Young, and C. R. Dean, Tuning superconductivity in twisted bilayer graphene, Science **363**, 1059 (2019).

[81] C. Heil, S. di Cataldo, G. B. Bachelet, and L. Boeri, Superconductivity in sodalite-like yttrium hydride clathrates, Phys. Rev. B **99**, 220502 (2019).

[82] I. A. Troyan, D. V. Semenok, A. G. Kvashnin, A. V. Sadakov, O. A. Sobolevskiy, V. M. Pudalov, A. G. Ivanova, V. B. Prakapenka, E. Greenberg, A. G. Gavriliuk, V. V. Struzhkin, A. Bergara, I. Errea, R. Bianco, M. Calandra, F. Mauri, L. Monacelli, R. Akashi, and A. R. Oganov, Anomalous high-temperature superconductivity in YH_6, Adv. Mater.**33**, 2006832 (2021).

[83] P. P. Kong, V. S. Minkov, M. A. Kuzovnikov, S. P. Besedin, A. P. Drozdov, S. Mozaffari, L. Balicas, F. F. Balakirev, V. B. Prakapenka, E. Greenberg, D. A. Knyazev, and M. I. Eremets, Superconductivity up to 243 K in yttrium hydrides under high pressure, arXiv:1909.10482.

[84] A. P. Drozdov, P. P. Kong, V. S. Minkov, S. P. Besedin, M. A. Kuzovnikov, S. Mozaffari, L. Balicas, F. F. Balakirev, D. E. Graf, V. B. Prakapenka, E. Greenberg, D. A. Knyazev, M. Tkacz, and M. I. Eremets, Superconductivity at 250 K in lanthanum hydride under high pressures, Nature (London) **569**, 528 (2019).

[85] A. D. Grockowiak, M. Ahart, T. Helm, W. A. Coniglio, R. Kumar, M. Somayazulu, Y. Meng, M. Oliff, V. Williams, N. W. Ashcroft, R. J. Hemley, and S. W. Tozer, Hot hydride superconductivity above 550 K, arXiv:2006.03004.

[86] T. Pandey and G. Y. Chitov, Phase diagram and topological order in the modulated XYZ chain with magnetic field, Phys. Rev. B **102**, 054436 (2020).

[87] A. A. Patel and S. Sachdev, Theory of a Planckian Metal, Phys. Rev. Lett. **123**, 066601 (2019).

[88] G. E. Volovik, Flat band and Planckian metal, JETP Lett. **110**, 352 (2019).